Role of pH in the hydrothermal synthesis of phase pure alpha Bi_2O_3 nanoparticles and its structural characterization

M. Malligavathy[1], D. Pathinettam Padiyan[1*]

Department of Physics, Manonmaniam Sundaranar University, Tirunelveli, Tamil Nadu, 627012, India

[*]Corresponding author, Tel: (+91) 9442063155; Fax: (+91) 2334363; E-mail: dppadiyan@msuniv.ac.in

Received: 30 March 2016, Revised: 17 September 2016 and Accepted: 30 November 2016

DOI: 10.5185/amp.2017/112
www.vbripress.com/amp

Abstract

Phase pure bismite nanoparticles were successfully prepared by means of hydrothermal method by varying the precursor solution pH from 10 to 13. The as-prepared nanoparticles were characterized by different techniques such as X-ray diffraction pattern (XRD), Raman spectroscopy, Scanning electron microscopy (SEM) and Energy dispersive X-ray spectroscopy (EDX). The effects of pH on the structural properties of these nanoparticles were corroborated using XRD and Raman spectrum. From the XRD pattern it is found that all the samples are polycrystalline in nature and the Raman spectra are used to confirm the phase transformation of the Bi_2O_3 nanoparticles. At the low pH value, the SEM image reveals that as-prepared samples are homogeneous with particle size of ~ 25 nm and with the increase in the pH value spherical particle forms uniform blocks like morphology for both the samples prepared at the pH 12 and 13. Copyright © 2017 VBRI Press.

Keywords: α-Bismuth oxide, hydrothermal method, structural properties, X-ray diffraction, Raman spectroscopy.

Introduction

Bismuth oxide (bismite) is a well-known metal oxide and it has been widely used due to its significant values of band gap, refractive index **[1]**, polarization of Bi^{3+} cation **[2]** and good electrochemical stability **[3, 4]**. These properties make bismuth oxide one of the most promising materials for the application in antireflective coating, sensors, fuel cells and solar cells **[5, 6, 7]**. Bi_2O_3 consists of five polymorphs such as α, β, γ, δ and ω-Bi_2O_3 **[8].** Among these, low temperature α-phase & high temperature δ-phase are stable and the remaining three polymorphs are high temperature metastable phases **[9]**. Each polymorph possesses different crystal structure and physical properties **[3, 9]**. Bismuth oxide nanoparticles were prepared by different methods like hydrothermal **[10, 11],** vapor-phase transport method **[12],** vapour phase deposition method **[13]** and so on. S. Hariharan et.al prepared α-Bi_2O_3 microrods through simple chemical method and studied its optical properties using UV-Vis absorption and photoluminescence spectra **[14].** Yi Wang et.al fabricated metastable tetrahedral γ-Bi_2O_3 using one step precipitation method and discussed its phase transition and photoluminescence spectra with the assistance of polyethylene glycol **[15]**. Ya-Jing Huang *et. al* synthesized bismuth coordinated polymer by hydrothermal method. After calcinations the samples are completely transformed into α-Bi_2O_3 and the photocatalytic degradation also explained **[16]**. Up to our knowledge, no data had been reported on the role of pH in the preparation of phase pure α-Bi_2O_3 nanoparticles using hydrothermal technique. In the present paper the structural and morphological properties of Bi_2O_3 nanoparticles prepared by hydrothermal method are investigated and discussed

Experimental

Materials/ chemicals details

Bismuth (III) nitrate pentahydrate (Merck, 99.9 %, Mumbai), sulfuric acid (RANKEM, 69 % GR, UN) and sodium hydroxide (Merck, 99.9 %, Mumbai) were purchased and used for the sample preparation. Double distilled water was used throughout the experiment.

Material synthesis / Reactions

Bismuth oxide nanoparticles were prepared by hydrothermal method using bismuth nitrate as a precursor. 0.02 M of $Bi(NO_3)_3.5H_2O$ was dissolved in 1.12 M of sulfuric acid (0.4 ml) and 39.6 ml of double distilled water was added to the above solution. After obtaining a clear solution, 0.2 M of sodium hydroxide (NaOH) was added in drops with continuous stirring until the pH reaches 10 and the solution was stirred for 2 h. Now the resulting solution was transferred into a 50 ml Teflon-lined stainless steel autoclave and hydrothermally treated at 120˚C in an oven for 6 h. Finally the autoclave was cooled to room temperature, the precipitates were centrifuged and washed several times using double distilled water. The resulting precipitates were dried overnight in an oven at 80˚C and the sample was named as B10. Similarly the samples were hydrothermally

treated by varying the pH (11, 12 and 13) of the precursor solution by adding NaOH and named as B11, B12 and B13 respectively.

Formation of Bi_2O_3 nanoparticles

Initially the Bi^{3+} ions created by hydration reacted during the hydrolysis process. Hence, bismuth hydroxide was formed in the first phase of reaction mechanism. Then in the second phase of reaction mechanism, the condensation of OH groups proceeds and it accompanied by the formation of bismuth oxide. In particular, the second step is strongly dependent on the pH in the reaction. The formation of Bi_2O_3 species is catalyzed by OH anions and proceeds through the formation of oxo-ligands which are stable at pH ≥12 **[17].**

Characterizations / Device fabrications /Response measurements

X-ray diffraction was performed on a PANalytical XPERT-PRO X-ray diffractometer with CuK_α (λ = 1.5406 Å) as an incident radiation. The accelerating voltage and current was 40 kV and 30 mA respectively. The surface morphology and composition were observed by a High Resolution Scanning Electron Microscope (FEI Quanta FEG 200) equipped with an Energy Dispersive X-ray spectroscopy (EDX). The Raman spectrum was recorded using a BRUKER RFS 27: Stand alone FT-Raman Spectrometer.

Results and discussion

X-ray diffraction

The XRD pattern of the samples prepared for the pH of 10, 11, 12 and 13 are shown in **Fig 1a, b, c** and **d** respectively.

From the XRD pattern it is found that, all the four samples are polycrystalline in nature. No diffracted peaks concerning Bi are noticed in the XRD pattern. The lattice parameters are obtained using "UNIT CELL" software. For sample B10, all the diffraction peaks belongs to bismuth hydroxide and there is no standard JCPDS pattern reported for bismuth hydroxide. Hence, the observed peaks are indexed using the software DICVOL 06. The peaks obtained are indexed to tetragonal phase with lattice constants a = b = 3.8673 (2) Å and c = 13.731 (2) Å. At pH = 11, the sample exhibits the mixture of α, γ-Bi_2O_3 and Bi_2O_4. Here the maximum intensity peak belongs to α-Bi_2O_3 phase is observed at the diffraction angle of 2θ = 33.26˚ while the second peak at 2θ = 27.39˚ belongs to γ-Bi_2O_3 phase. All the peaks are in agreement with the JCPDS data file number 76-1730 (α-Bi_2O_3) and 71-0467 (γ-Bi_2O_3). In addition to these peaks another peak observed at 2θ value 23.84˚ corresponds to the plane (-1 1 1) of Bi_2O_4 (JCPDS: 83-0410). The lattice parameter values of α-Bi_2O_3 (monoclinic) are a = 5.838 (1) Å, b = 7.986 (8) Å, c = 7.609 (4) Å, cell volume = 326.1 (2) $(Å)^3$ and for γ-Bi_2O_3 (cubic), a = b = c = 10.2543 (4) Å, cell volume = 1078.2 (1) $(Å)^3$ which is in agreement with the standard lattice parameter values in the JCPDS file.

The XRD pattern of the system B12 is shown in **Fig. 1c** and it is found to have a mixture of two phases. Most of the observed X-ray peaks (except four peaks) are matched to α-Bi_2O_3 with JCPDS card number 76-1730 with lattice constants, a = 5.8405 (6) Å, b = 8.254 (1) Å, c = 7.330 (1) Å & cell volume = 328.57 (6) $(Å)^3$. The peaks at 2θ value 23.90˚, 29.47˚, 30.15˚ and 38.74˚ correspond to the planes (-1 1 1), (-3 1 1), (4 0 0) and (-3 1 2) of Bi_2O_4 respectively and are in agreement with the JCPDS data file number 83-0410. It is clear that, the metastable γ-Bi_2O_3 changed gradually into α-Bi_2O_3 as the pH increased. At pH = 13, all the X-ray peaks coincides with α-Bi_2O_3 of monoclinic phase and the lattice parameters are a = 5.8349(4) Å, b = 8.1363(6) Å, c = 7.5014 (8) Å. This is in agreement with the JCPDS data file number 76-1730 of Bi_2O_3 which crystallizes in the monoclinic system.

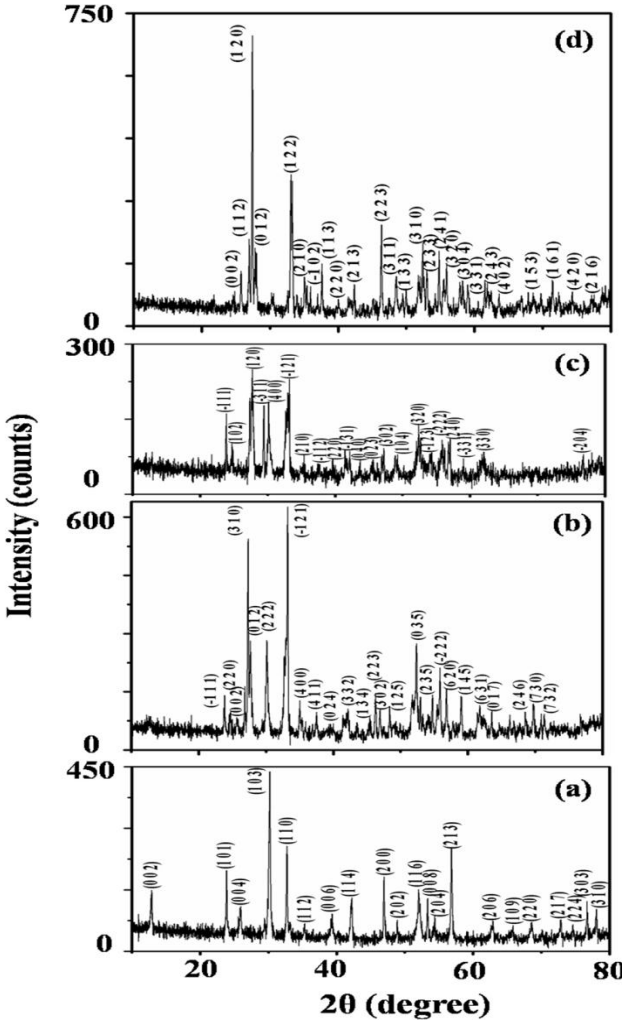

Fig. 1. XRD pattern of the nanoparticles prepared at the pH of (a) 10 (b) 11 (c) 12 and (d) 13.

All the sharp peaks reveal a high degree of crystallization and the peaks due to the impurity phases diminished with increase in pH value. No other X-ray peaks are observed, indicating the high purity of the α-Bi_2O_3 samples prepared at the pH of 13. The pH of the precursor solution have a great influence on the crystal

structure of the as-prepared samples and our results show that, pure bismuth hydroxide can be obtained at the pH of 10 and phase pure α-Bi_2O_3 at the higher pH of 13. The crystallinity increases with the increase in pH value except for pH 12 which is attributed to the mixed phase. Moreover, XRD clearly shows that among the four samples B13 **(Fig 1d)** have the highest crystallinity and the peaks intensities are higher. When the reaction was performed in the presence of a strong alkali medium, more number of hydroxide ions firstly reacts with Bi^{3+} to give bismuth hydroxide, which then gets dehydrated to form α-Bi_2O_3.

The crystallite size of the samples are calculated using Scherrer's formula,

$$D = K\lambda/\beta cos\theta \quad (1)$$

where, K - constant, usually equal to 0.9, λ - wavelength of X-ray, β - full width at half maximum and θ - Bragg's angle.

The crystallite size is calculated for all the samples by considering the first prominent peak and the values are 58, 51, 23 and 45nm for pH 10, 11, 12 and 13 respectively. The crystallite size decreases from 58 nm as pH increases up to the pH value of 12 and then it increases to 45 nm for the highest pH. At pH 11 to 12, phase change have occurred during the hydrothermal process, which causes the crystallite size becoming small. On increasing the pH from 12 to 13 the crystallite size increases which may be associated with the faster growth of the nanoparticles **[18]**.

Raman analysis

Raman analysis is used to confirm the phase transformation of the Bi_2O_3 nanoparticles synthesized by hydrothermal method. A comparative structural study has been made on the nanoparticles prepared with the pH 10, 11, 12 and 13. The Raman bands are of four types: acoustic Raman peaks in the low frequency (less than 100 cm^{-1}), heavy metal peaks in the region (70-160 cm^{-1}), bridged anion peaks at the intermediate region (300-600 cm^{-1}) and non-bridged anion peaks at higher frequencies **[19, 20].** In the Raman spectra the bands from 0 to 1000 cm^{-1} of crystalline Bi_2O_3 can be divided into three regions (i) bands in the region of 0-300 cm^{-1} are derived from both acoustic Raman and heavy metal modes **[21]** (ii) the band from 300-600 cm^{-1} are assigned to symmetric stretching anion motion in an angularly constrained Bi-O-Bi configuration from BiO_6 octahedral units **[22]** (iii) the region of 600-1000 cm^{-1} are assigned to Bi-O stretching vibrations **[23].**

Fig. 2 displays the Raman spectra for the samples prepared at the pH of 10 and 11. In the region below 120 cm^{-1} and above 150 cm^{-1} are mainly attributed to vibration modes of heavy elements such as bismuth or lattice vibrations and oxygen vibrations. The Raman bands with frequencies above 150 cm^{-1} are very broad in comparison with the band below 120 cm^{-1} which gives evidence for the strong anharmonicity of O modes **[24].** The peaks observed at 412, 529 and 628 cm^{-1} in **Fig. 2**(a) are confirming the presence of bismuth hydroxide **[25]** which is in agreement with the XRD pattern.

With the increase in pH from 10 to 11, the intensity of Raman peaks get increased which is in agreement with the XRD results and the peaks obtained are due to the mixed phase of α and γ-Bi_2O_3. From this it is clear that, increase in pH value leads to the structural transformation. Raman features in the range of 50-600 cm^{-1} and 50-900 cm^{-1} have been assigned to α and γ-Bi_2O_3 respectively **[26].** The Raman bands at 62 and 87 are assigned to A_g and B_g vibration modes of Bi in Bi_2O_3 **[24, 27].** However the appearance of the peaks at 62, 87, 206, 277, 456, 537 and 622 cm^{-1} in the Bi_2O_3 system can also be assigned to the presence of α-Bi_2O_3 as evident in the XRD studies **[28, 29, 30]** which are attributed to displacement of the O atoms with respect to the Bi atoms causing Bi-O elongation **[24, 30].**

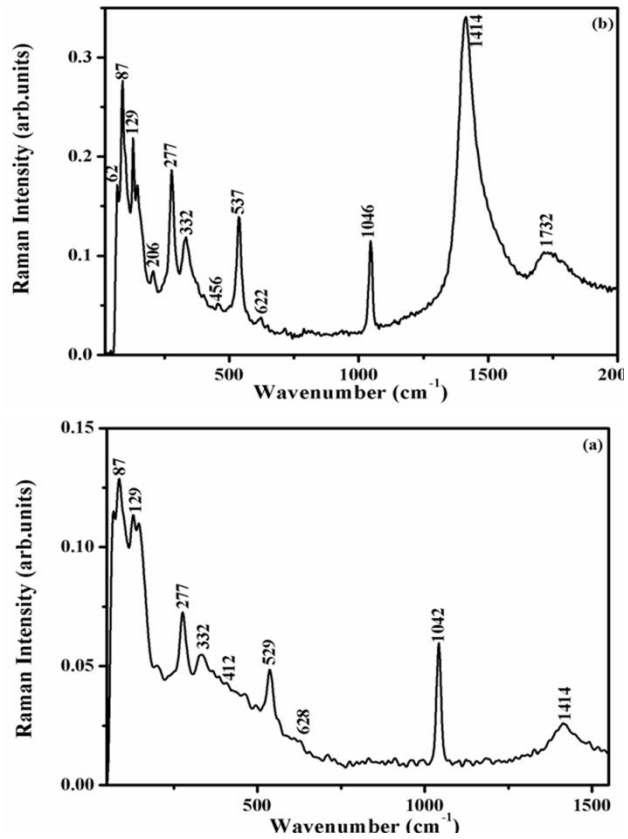

Fig. 2. Raman spectra of the samples prepared at the pH of (a) 10 and (b) 11.

The Raman spectrum **Fig 3(a)** and **(b)** presents Raman peaks that can be attributed to the α-Bi_2O_3 phase. All the peaks agreed well with the literature which further confirms that the nanoparticles are composed of monoclinic α-Bi_2O_3. Most of the peaks above 120 cm^{-1} can be assigned to (A_g, B_g) modes of α-Bi_2O_3 **[24].** The Raman bands observed in the range of 120-150 cm^{-1} are due to the displacement of both Bi and O atoms. The Raman absorption observed in the spectral region of 100 – 200 cm^{-1} has been attributed to Bi^{3+}-O vibrations in BiO_6 octahedral **[31].** The peaks observed at 68, 70, 85,

117, 120, 135, 138, 153, 162, 184, 212, 282, 285, 408, 414, 418, 448, 470, 524 and 630 cm^{-1} are assigned to the presence of α-Bi_2O_3. The mode 119 cm^{-1} is coming from A_g symmetry and mode 138 may come from the displacements of both Bi and O atoms in the α-Bi_2O_3 lattice **[32, 33].**

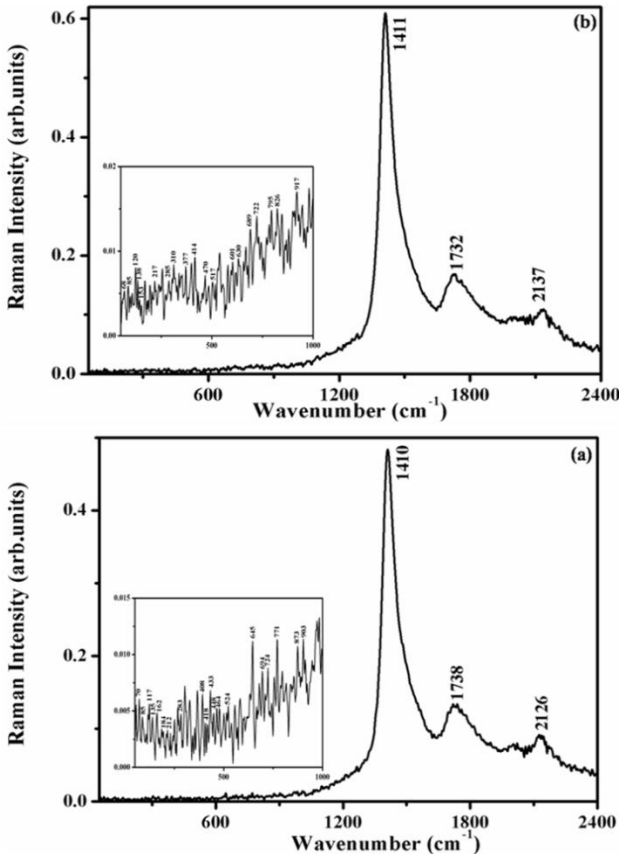

Fig. 3. Raman spectra of the samples prepared at the pH of (a) 12 and (b) 13 and the inset figure shows the peaks observed in the range of 50-1000 cm^{-1}

The band from 377 cm^{-1} is assigned to the Bi-O-Bi stretching vibrations of distorted BiO_6 octahedral units and the small bands in the region 520-590 cm^{-1} are associated with the presence of Bi^{3+} and oxygen vacancies. The low shoulder around 601 cm^{-1} is assigned to Bi-O stretching vibrations of BiO_6 octahedral units **[32, 34].** When the pH changes from 12 to 13, some bands are shifted towards the lower frequency. The shifting of the band to 310 and 520 cm^{-1} shows the introduction of non-stoichiometry in α-Bi_2O_3 lattice with the insertion of oxygen **[35].** Consequently with increase in pH value, the distortion on the octahedral structure increases which shift the Bi-O stretching mode 281 cm^{-1} to higher wave number **[36].** Thus, the results of Raman spectra are in agreement with the XRD results. The Raman bands and their assignment are given in **Table 1**.

SEM analysis

The morphology of the samples are observed using field emission scanning electron microscope. **Fig 4** shows the close up view on morphology of the samples synthesized

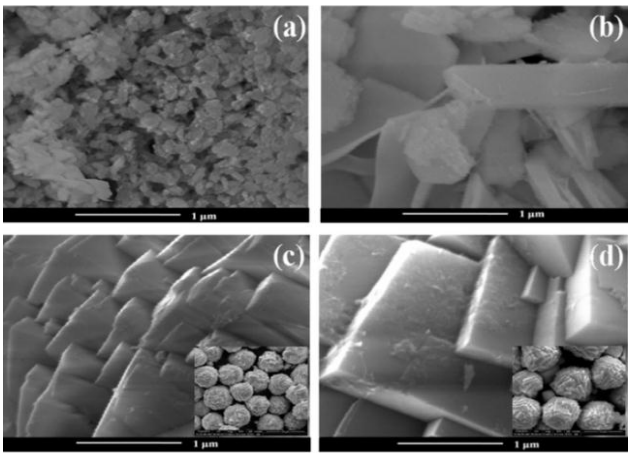

Fig. 4. HR-SEM images of the nanoparticles prepared at the pH of (a) 10 (b) 11 (c) 12 and (d) 13.

Table 1. The Raman bands and their assignment.

Wave number (cm^{-1})	Band assignment
100 - 200	Bi^{3+}-O vibrations in BiO_6 octahedra
120 - 150	displacement of bismuth and oxygen atoms
300 - 600	symmetric stretching anion motion in an angularly
BiO_6 octahedral units 600 - 1000	Bi-O stretching vibrations

at different pH values with the magnification of 50,000. In B10, **Fig. 4(a)** most of the grains are homogeneous with individual particles of size approximately 25 nm and there is no agglomeration occurred. However, bismuth hydroxide powders also have few larger particles of irregular shapes.

The variation of morphology with pH **Fig. 4(a)** to **Fig. 4(b),** shows the formation of impurity phases and the shape of the aggregated particles is mainly platelets like structure. **Fig 4 (c)** shows that the sample prepared at pH 12 composed of large quantity of uniform square blocks (see inset). Each sphere blocks contains uniform geometrical shaped particles with an average diameter of 1 μm. When the pH value increases from 12 to 13, regular morphology is observed and the sizes of the blocks are larger **(Fig. 4(d))** compared to **Fig. 4(c)**. The growth of the large square blocks is usually preferred in the hydrothermal synthesized Bi_2O_3 nanoparticles. Moreover, in our present study it is found that the pH value of the precursor has an obvious effect on the morphology of Bi_2O_3 nanoparticles. NaOH selected to change the solutions pH, prevents the agglomeration between the particles during the formation of nanoparticles. EDAX analysis shows that Bi_2O_3 consists of Bi and O element and no other impurities are present which confirms the purity of the samples.

Conclusion

In summary, Bi_2O_3 nanoparticles were synthesized from a solution of bismuth nitrate pentahydrate in sodium hydroxide using simple hydrothermal process at the temperature of 120 ºC by varying the pH from 10 to 13. The effects of pH on the structural and morphological properties of Bi_2O_3 were investigated in the current study. The XRD pattern indicated that the samples prepared at the pH 13 were in pure monoclinic form with the existence of higher degree crystallinity. Scanning electron microscope analysis indicated that the surface morphology varied with the pH. With the increase in pH, the morphology of the as-prepared samples transformed progressively from homogeneous particles to spherical blocks. At pH 10, the bismuth hydroxide obtained showed that the grains were homogeneous. The mixture of α-Bi_2O_3/γ-Bi_2O_3/Bi_2O_4 and α-Bi_2O_3/Bi_2O_4 obtained at pH 11 and 12, yielded plates and spherical blocks with diameter of 1 micrometer. α-Bi_2O_3 nanoparticles obtained at pH 13 consisted of spherical blocks of various sizes. Raman spectroscopy was used to monitor the structural changes that occur in the hydrothermal process and the bismuth hydroxide to bismuth oxide transformation was due to the condensation of Bi-OH to Bi-O-Bi. Hence, it is concluded that the pH plays an important role in deciding the structural and morphological properties of the samples.

Acknowledgements

One of the authors M. Malligavathy would like to thank UGC, New Delhi for BSR fellowship. The authors thank SAIF, IIT Madras for recording Raman and HR-SEM measurement.

References

1. Leontie, L.; Caraman, M.; Visinoiu, A.; Rusu, G.I; *Thin Solid Films*., **2005**, *473*, 230. **DOI**: 10.1016/j.tsf.2004.07.061
2. Dimitrov, V.; Sakka. S; *J. Appl. Phys.*,**1996**, *79*, 1736. **DOI**: 10.1063/1.360962
3. Gobrecht, H.; Seeck, S.; Bergt, H.E.; Martens, A.; Kossmann, K; *Phys. Stat. Sol*., **1969**, *33*, 599. **DOI**: 10.1002/pssb.19690330213
4. Dolocan, V; *Appl. Phys*., **1978**, *16*, 405. **DOI**: 10.1007/BF00885866
5. Arya, S.; Singh, H.; *Thin Solid Films*., **1979**, *62*, 353. **DOI**: 10.1016/0040-6090(79)90010-5
6. Hyodo, T.; Kanazawa, E.; Takao, Y.; Shimizu, Y.; Egashira, M; *Electrochemistry*., **2000,** *68*, 24. **ISSN**: 1344-3542
7. Sammes, N. M.; Tompsett, G. A.; Nafe, H.; Aldinger, F*; J. Eur. Ceram. Soc*., **1999**, *19*, 1801. **DOI**: 10.1016/S0955-2219(99)00009-6
8. Shuk, P.; Wiemhofer, H.D.; Guth, U.; Gopel, W.; Greenblatt, M; *Solid State Ionics.*, **1996**, *89*, 179. **DOI**: 10.1016/0167-2738(96)00348-7
9. Gualtieri, A.F.; Immovilli, S.; Prudenziati, M; *Powder Diffraction*., **1997**, *12*, 90. **ISSN**: 0885-7156
10. Jungang Hou; Chao Yang; Zheng Wang; Weilin Zhou; Shuqiang Jiao; Hongmin Zhu; *Appl. Catal., B: Environ*., **2013**, *142*, 504. **DOI**: 10.1016/j.apcatb.2013.05.050
11. Ying Xiong; Mingzai Wu; Jing Ye; Qiannwang Chen.; *Mater. Lett*., **2008,** *62*, 1165. **DOI**: 10.1016/j.matlet.2007.08.004
12. Ling, B.; Sun, X.W.; Zhao, J.L.; Shen, Y.Q.; Dong, Z.L.; Sun, L.D.; Li, S.F.; and Zhang, S*; J. Nanosci. Nanotechnol.*, **2010,** *10*, 8322. **DOI**: 10.1166/jnn.2010.3051
13. Latha Kumari; Jin-Han Lin and Yuan-Ron Ma.; *Nanotech.*, **2007**, *18*, 295605. **DOI**: 10.1088/0957-4484/18/29/*295605*
14. Hariharan, S.; Udayabhaskar, R.; Ravindran, T.R.; Karthikeyan, B; *Spectrochim Acta Part A: Mol. Biomol. Spectrosc*., **2016,** *163*, 13. **DOI**: 10.1016/j.saa.2016.02.045
15. Yi Wang; Yunling Li.; *J. Colloid Interface Sci*., **2015,** *454*, 238. **DOI**: 10.1016/j.jcis.2015.05.001
16. Ya-Jing Huang; Yue-Qing Zheng; Hong-Lin Zhu; Jin-Jian Wang.; *J. Solid State Chem.*, **2016,** *239*, 274. **DOI**: 10.1016/j.jssc.2016.05.006
17. Eva Bartonickova; Jaroslav Cihlar; Klara Castlova.; *Process. Appl. Ceram.*, **2007**, *1*, 29. **DOI**: 10.2298/PAC0702029B
18. Sadhana, K.; Naina Vinodini, S.E.; Sandhya, R.; Praveena, K; *Adv. Mater. Lett*., **2015**, *6*, 717. **DOI**: 10.5185/amlett.2015.5874
19. Lines, M.E; *J. Non-Cryst. Solids.*, **1987,** *89*, 143. **DOI**: 10.1016/S0022-3093(87)80329-0
20. Lines, M.E.; Miller, A.E.; Nassau, K.; Lyons, K.B; *J. Non-Cryst. Solids.*, **1987**, *89*, 163. **DOI**: 10.1016/S0022-3093(87)80330-7
21. Rao, G.S.; Veeraiah, N; *J. Alloys Compd*., **2001,** *327*, 52. **DOI**: 10.1016/S0925-8388(01)01559-6
22. Hazra, S.; Mandal, S.; Gosh, A; *Phys. Rev B*., **1997**, *56*, 8021. **DOI**: 10.1103/PhysRevB.56.8021
23. Sreenivasu, D.; Chandramouli, V; *Bull. Mater. Sci.*, **2000**, *23*, 281. **DOI**: 10.1007/BF02720083
24. Denisov, V.N.; Ivlev, A.N.; Lipin, A.S.; Mavrin, B.N.; and Orlov, V.G; *J.Phys.: Condens. Matter*., **1997**, *9*, 4967. **DOI**: 10.1088/0953-8984/9/23/020
25. Vivier, V.; Regis, A.; Sagon, G.; Nedelec, J.Y.; Yu, L.T.; Cachet-Vivier, C; *Electrochim. Acta*., **2001**, *46*, 907 **DOI**: 10.1016/S0013-4686(00)00677-0
26. Baia, L.; Stefan, R.; Kiefer, W.; and Simon, S; *J. Raman Spectrosc*., **2005**, *36*, 262. **DOI**: 10.1002/jrs.1306
27. Kumari, L.; Lin, J.; and Ma, Y; *J.Phys.: Condens.Matter*., **2007,** *19*, 11. **DOI**: 10.1088/0953-8984/19/40/406204
28. Franklin, D; *J. Solid State Chem*., **1992**, *97*, 319. **DOI**: 10.1016/0022-4596(92)90040-3
29. Bourja, L.; Bakiz, B.; Benlhachemi, A.; Ezahri, M.; Valmalette, J.C.; Villain, S.; Gavarri, J.R; *Adv. Mater. Sci. Eng*., **2009**, 1. **DOI**: 10.1155/2009/502437
30. Maria Vila; Carlos Diaz-Guerra; Katharina Lorenz; Javier Piqueras; Eduardo Alves; Silvia Nappini and Elena Magnano; *J. Mater. Chem. A.*, **2013**, *1*, 7920. **DOI**: 10.1039/C3TA11342F
31. Betsch, R.J.; and White, W.B.; *Spectrochim. Acta, Part A*., **1978,** *34*, 505. **DOI**: 10.1016/0584-8539(78)80047-6
32. Gondal, M.A., Tawfik A.Saleh.; and Q. Drmosh; *Sci. Adv. Mater*., **2012**, *4*, 1. **DOI**: 10.1166/sam.2012.1310
33. Ling, B.; Sun, X.W.; Zhao, J.L.; Shen, Y.Q.; Dong, Z.L.; Sun, L.D.; Li, S.F.; and Zhang, S; *J. Nanosci. Nanotechnol*., **2010**, *10*, 8322. **PMID**: 21121334
34. Ardelean, I.; Todor, I.; Pascuta, P; *Mod. Phys. Lett B*., **2004**, *18*, 275. **DOI**: 10.1142/S0217984904006792
35. Ho, C.H.; Chan, C.H.; Huang, Y.S.; Tien, L.C.; Chao, L.C; *Opt. Express*., **2013,** *21*, 11965. **DOI**: 10.1364/OE.21.011965
36. Franklin D. Hardcastle and Israel E. Wachs; *J. Solid State Chem.*, **1992**, *97*, 319. **DOI**: 10.1016/0022-4596(92)90040-3

